

ZTF SN Ia DR2: Study of Type Ia Supernova lightcurve fits

Rigault, M.^{1*}, Smith, M.^{1,2}, Regnault, N.³, Kenworthy, W. D.⁴, Maguire, K.⁵, Goobar, A.⁴, Dimitriadis, G.⁵, Johansson, J.⁴, Amenouche, M.⁶, Aubert, M.⁷, Barjou-Delayre, C.⁷, Bellm, E. C.⁸, Burgaz, U.⁵, Carreres, B.^{9,10}, Copin, Y.¹, Deckers, M.⁵, de Jaeger, T.³, Dhawan, S.¹¹, Feinstein, F.⁹, Fouchez, D.⁹, Galbany, L.^{12,13}, Ginolin, M.¹, Graham, M. J.¹⁴, Kim, Y.-L.², Kowalski, M.^{15,16}, Kuhn, D.³, Kulkarni, S. R.¹⁴, Müller-Bravo, T. E.,^{12,13} Nordin, K.¹⁶, Popovic, M.¹, Purdum, J.¹⁷, Rosnet, P.⁷, Rosselli, D.⁹, Racine, B.⁹, Ruppin, F.¹, Sollerman, J.¹⁸, Terwel, J. H.^{5,19}, and Townsend, A.¹⁶

(Affiliations can be found after the references)

ABSTRACT

Type Ia supernova (SN Ia) cosmology relies on the estimation of lightcurve parameters to derive precision distances that leads to the estimation of cosmological parameters such as H_0 , Ω_M , Ω_Λ and w . The empirical SALT2 lightcurve modeling that relies on only two parameters, a stretch x_1 , and a color c , has been used by the community for almost two decades. In this paper we study the ability of the SALT2 model to fit the nearly 3000 cosmology-grade SN Ia lightcurves from the second release of the Zwicky Transient Facility (ZTF) cosmology science working group. While the ZTF data was not used to train SALT2, the algorithm is modeling the ZTF SN Ia optical lightcurves remarkably well, except for lightcurve points prior to -10 d from maximum, where the training critically lacks statistics. We find that the lightcurve fitting is robust against the considered choice of phase-range, but we show the $[-10; +40]$ d range to be optimal in terms of statistics and accuracy. We do not detect any significant features in the lightcurve fit residuals that could be connected to the host environment. Potential systematic population differences related to the SN Ia host properties might thus not be accountable for by the addition of extra lightcurve parameters. However, a small but significant inconsistency between residuals of blue- and red-SN Ia strongly suggests the existence of a phase-dependent color term, with potential implications for the use of SNe Ia in precision cosmology. We thus encourage modellers to explore this avenue and we emphasize the importance that SN Ia cosmology must include a SALT2 retraining to accurately model the lightcurves and avoid biasing the derivation of cosmological parameters.

Key words. ZTF ; Cosmology ; Type Ia Supernovae

1. Introduction

Type Ia supernovae (SNe Ia) are standardizable cosmological candles. With a limited set of parameters, usually derived from lightcurve observations, one can derive relative distances at a precision of about 7% up to a few Gpc thanks to their remarkable brightness at optical wavelengths (< -19 mag). These characteristics make SNe Ia a key cosmological tool to probe the expansion history of our Universe, and lead to the discovery of the acceleration of its expansion (Perlmutter et al. 1999; Riess et al. 1998), see (Goobar & Leibundgut 2011) for a review, and play a central role for the derivation of the Hubble-Lemaître constant, which value is currently highly debated (Planck Collaboration et al. 2020; Freedman et al. 2019; Riess et al. 2022).

For the last 25 years, two lightcurve parameters have been used to standardize SNe Ia (Tripp 1998), exploiting two empirical relations: redder SNe Ia are fainter (color yields to the redder-fainter relation; Riess et al. 1996) and slower evolving SNe Ia are brighter (stretch yields to the brighter-slower relation; Phillips 1993). Accounting for these two linear relations reduces the natural SN Ia Hubble diagram dispersion from 0.40 mag to 0.15 mag (e.g., recent SN Ia compilations Betoule et al. 2014; Scolnic et al. 2018; Brout et al. 2022). Half of this variance could be explained by measurement or modeling errors, leaving ~ 0.10 mag unexplained and usually referred to as the intrinsic scatter.

The stretch and color lightcurve parameters are derived using lightcurve fitter algorithms and SALT2 has been the community

standard for the last decade (Guy et al. 2007, 2010; Betoule et al. 2014). This data-driven model is based on a principal component analysis (PCA) with an exponential phase-independent color-law. The PCA and color-law parameters are trained on calibrated lightcurves and spectra to build a spectro-temporal model. The first component M_0 (eigenvalue x_0) corresponds to the spectral template for an average SN Ia, while the second M_1 (eigenvalue x_1) corresponds to phase and amplitude deformation of the M_0 component. The third component has been shown to contain insignificant information. The amplitude of the multiplicative color correction is called c . For SALT2, x_1 corresponds to the stretch, x_0 to the amplitude (flux), and c to the color. The SN lightcurve shape is therefore captured using only two parameters x_1 and c . The most used SALT2 training is that from Betoule et al. (2014) and is usually referred to as SALT2.4. Taylor et al. (2021) provide a recent retraining of SALT2.4 with additional data. Kenworthy et al. (2021) re-designed the original SALT software and trained it with a recent SN Ia cosmological compilation (Scolnic et al. 2018) and released it as SALT3. Some SALT alternatives exist with 2-components such as MLCS (Jha et al. 2007), SNooPy (Burns et al. 2011), BayesSN (Mandel et al. 2022; Grayling et al. 2024) and PISCOLA (Müller-Bravo et al. 2022) that predominately differ from SALT by incorporating additional physics, most notably in the treatment of dust reddening.

Yet, the stretch and color standardized SN Ia magnitudes have been shown to significantly depend on their host-environments. SNe Ia from massive host galaxies or redder environments are brighter (after standardisation) than those from

* Corresponding author: m.rigault@ip2i.in2p3.fr

lower-mass (bluer) hosts (e.g., Sullivan et al. 2010; Roman et al. 2018; Rigault et al. 2015, 2020; Briday et al. 2022). This is usually referred to as the “mass-step” as it was first observed using global host stellar mass tracers (Kelly et al. 2010; Sullivan et al. 2010). The actual origin of this effect is highly debated as either caused by differences in progenitor age “prompt vs. delayed” (Rigault et al. 2013, 2020; Roman et al. 2018; Briday et al. 2022) or as originating from dust color-law variation between environments (Brout & Scolnic 2021; Popovic et al. 2021). It is possible that both are true, or that both are related aspects of a one underlying parameter (Wiseman et al. 2022; Kelsey et al. 2023). In any case, understanding the origin of these correlations is important, as any differences in their evolution with redshift is likely to impact the inferred cosmological parameters.

An ideal solution would be to find signs of such a SN-host correlation directly in the SN Ia lightcurves. As such, one could empirically correct for it as one does for the stretch and color, hoping to capture the entire SN Ia magnitude variance. In that context, alternative SN Ia models have emerged. Saunders et al. (2018) and Léget et al. (2020) derived spectroscopic information, such as silicon velocities and equivalent widths at maximum light, to standardize SNe Ia using this information instead of the stretch. They were able to reach ~ 0.15 mag dispersion with five or more parameters, but did not see a significant reduction in the Hubble diagram scatter and are still affected by significant environmental biases. A promising avenue is the twin-technique. Introduced by Fakhouri et al. (2015) based on the spectro-photometric Nearby Supernova Factory sample (SNfactory; Aldering et al. 2002), the idea is that two SNe Ia having nearly identical spectral time-series should have intrinsically similar absolute brightness. Advances of machine learning methods enabled Boone et al. (2021a) and Boone et al. (2021b) to simplify the “twinning” down to three intrinsic parameters estimated near maximum light. They demonstrate that twinning, based on spectroscopy rather than lightcurve photometry, provides a scatter as low as ~ 0.07 mag leading to strong reduction, but not a full cancellation, of the astrophysical biases. However, acquiring spectro-photometry is difficult and this technique has not been demonstrated to work outside of the SNfactory sample in the very nearby Universe. Future space missions such as the Nancy Roman Space Telescope might be able to acquire such data, through slit-less spectroscopy, at high-redshifts (Rose et al. 2021; Rubin et al. 2022).

Twinning has nonetheless demonstrated that additional information is available in the SN data that is not yet captured by classical photometric lightcurve fitters. The question is whether one can identify such information in the phase-evolution of multi-band photometry or if this is solely accessible with spectroscopic data.

In this paper, we study the SN Ia lightcurve residuals of the second data-release of the Zwicky Transient Facility (ZTF, Bellm et al. 2019; Graham et al. 2019) cosmology science working group (“DR2”; Rigault et al. (a)). This release contains SN Ia lightcurves with daily cadence and unprecedented phase coverage. This dataset consequently is particularly well suited to probe deviations from the current lightcurve templates and unveil new features. Increased diversity has been observed at both early (~ 15 d prior to maximum light) and late-time (> 30 d after to maximum light), suggesting that these phases contain key information about SN Ia physics and its diversity (e.g. Dimitriadis et al. 2019; Deckers et al. 2022, 2023). With training samples dominated by high-redshift data around maximum light, this diversity is likely not encoded in the SALT2 model. The unique phase coverage of ZTF-Cosmo-DR2 allows to test how well this

model describes the SN Ia population as a function of phase, and hence to deduce the exact phase range that should be used for cosmological inference.

We start the paper with a short introduction of the “DR2” sample in Sect. 2. We then present the SN Ia SALT2 lightcurve residuals in Sect. 3. Observed lightcurve residual deviations are studied in detail in Sect. 4, notably variations as a function of lightcurve- and host-parameters. The robustness of the lightcurve parameter estimation released as part of the “DR2” is presented in Sect. 5. We conclude in Sect. 6.

Throughout the paper, except if explicitly mentioned otherwise, we referred to as phases “rest-frame” phases, i.e. rest-frame time, in days, with respect to the estimated maximum light “ t_0 ”.

2. ZTF Cosmology DR2

The second data-release of the ZTF Cosmology Science working group (“DR2”) is presented on Rigault et al. (a). It contains 3628 spectroscopically confirmed SNe Ia with a median redshift of $z = 0.08$. The lightcurves have a typical three day cadence in ztf:g (g) and ztf:r (r) and a five day cadence in ztf:i (i). Of these, 2625 are non-peculiar SNe Ia passing the “basic cuts” (“good sampling” and reasonable lightcurve fit parameters; see Rigault et al.). In the -10 to $+40$ rest-frame phase range, all have at least seven detection, two of which pre- and two other post-maximum light¹, and detections in at least two bands. Nearly half of our targets (46%) have i -band data.

Thanks to the unique ZTF cadence, the typical first detection is two weeks prior to maximum light, with 80% of our 2576 SNe Ia having at least one detection prior to -10 d. Considering the $[-20, +50]$ d phase range, our targets have on average 20 detections pre- and 50 post-maximum light. 85% have at least one detection past $+30$ d. Such unprecedented statistics makes the ZTF-Cosmo-DR2 dataset a unique opportunity to study SN Ia lightcurves in detail.

Except if mentioned otherwise, the default lightcurve filter algorithm is SALT2 (Guy et al. 2010), as made available in sncoo (Barbary et al. 2023). By default, we use the SALT2 version “T21” from Taylor et al. (2021), which corresponds to a small calibration update of the reference version 2.4 (Betoule et al. 2014). As explained in Sect. 3, the default fitted phase range is $\phi \in [-10, +40]$ d. See Rigault et al. (a) for details concerning the lightcurve extraction and fitting procedure.

3. Generic overview of SN Ia lightcurve fitting.

We summarize the lightcurve residuals for the 2625 SNe Ia from the DR2 sample in Fig. 1. The lightcurves are modeled as the best SALT2.4 (T21) lightcurve template fitted in the $\phi \in [-10, +40]$ d rest-frame phase-range on all three ZTF bands (see Sect. 4). This figure presents the normalized lightcurve residuals, i.e., the pull $\equiv (\text{data} - \text{model}) / \text{error}$ where errors are a quadratic sum of the actual statistical measurement errors, a model error (sub-dominant) and a filter-dependent error-floor, estimated as a fraction of the observed flux. This error-floor is estimated to get a pull normalized median absolute deviation (nMAD) of 1 for the fitted phase-range and corresponds to unaccounted for errors related to the forced photometry transient signal extraction. We find that g , r and i SN photometry need a 2.5%, 3.5%, and 6% error-floor respectively, in good agreement with simulations presented by Amenouche et al. as part of

¹ all but one have both g and r data, that one target has g and i but no r

the ZTF-Cosmo-DR2 release. As illustrated in Fig. 1, the full lightcurve error leads to an expected pull scatter of 1σ at all wavelengths (white bands). We emphasize that the add-on error-floor has no effect prior $\phi = -20$ d as there is no SN flux yet at those phases. In that figure, the residuals are binned per phase (1 d for g and r , 2 d for i). We display the median (used as a robust mean) residual per bin and compute its error as the error on the mean ($\text{nMAD}/\sqrt{N-1}$), with the nMAD used as a robust STD. The significance shown in Fig. 1 (and similar figures) corresponds to the deviation of the median from zero given its error.

The pre-explosion epochs $\phi < -20$ d is also interesting in that figure for two aspects. First, the $\phi[-50, -20]$ d phase range was not considered for forced-photometry baseline correction (see Smith et al.). Therefore, it allows us to test the quality of this procedure. We see in Fig. 1 that the residuals are indeed well centered on zero with a scatter of one, as it should. Second, since we see no significant excess in the $\phi[-40, -20]$ d period displayed in that figure, we can exclude the existence of systematic significant pre-explosion features.

At epochs following the explosion, one can notice many small to medium size deviations to the expected model as shown Fig. 1 These are discussed in detail in Sect. 4.

4. Study of the lightcurve residuals

At first glance, it is generally remarkable that the empirical SALT2 model, trained on a much smaller dataset than this ZTF data-release and made of SNe Ia at higher redshift, performs so well. That is particularly true near maximum light ($\phi \in [-5, +20]$ d), where most of the flux information is extracted to derive cosmological distances.

We first discuss residuals in characteristic epochs of the lightcurves in Sect. 4.1. We then investigate in Sect. 4.2 the impact of narrowing the fitted phase-range and discuss why we selected the $\phi \in [-10, +40]$ d phase-range for our baseline lightcurve fits in ZTF-Cosmo-DR2. We continue our investigation of the lightcurve residuals in Sect. 4.3 where we analyse how they vary as a function of SN parameters and then in Sect. 4.4 as a function of SN environmental properties.

4.1. Analysis of the main lightcurve epochs.

Figure 2 illustrates typical SN Ia lightcurves and SALT2 models using actual ZTF-Cosmo-DR2 data. SN Ia data shown in this figure are normalized by their best fitted flux at maximum light (x_0) and corrected for Milky Way extinction (Schlafly et al. 2011). For the sake of visibility, it contains only targets within a $z \in [0.05, 0.09]$ redshift range, a color range of $c \in [-0.1, +0.1]$ and a stretch range $x_1 \in [-1, +1]$, such that all displayed SNe Ia are comparable. This figure illustrates three periods that we discuss in detail below: (1) early-phases, the first d following the explosion ($\phi \in [-18, -10]$ d); (2) the maximum light ($\phi \in [-5, +10]$ d); and (3) the second peak in the red- to near-infrared bands ($\phi \in [+15, +35]$ d) that is a noticeable SN Ia lightcurve feature.

4.1.1. Early phases: $\phi \in [-18, -10]$ d.

Early SN Ia epochs are well probed by ZTF. This period is particularly important for progenitor studies as it contains imprints of the progenitor channel(s) and early lightcurve excesses are particularly looked for (see e.g., Deckers et al. 2022, and refer-

ence therein), as well as the rising time (e.g., Firth et al. 2015). In turn, a deeper understanding of SN Ia physics provides key information for SN Ia cosmological analyses to understand and mitigate the origin of astrophysical biases.

However, this very early phase-range currently lacks training data and existing lightcurve fitting algorithms are mostly extrapolating below $\phi = -10$ d (see data made available by Guy et al. 2010; Betoule et al. 2014, Taylor et al. 2021 and Kenworthy et al. 2021). It is therefore not surprising to see strong deviations in this phase-range largely unexplored before ZTF. In Fig. 1, and in the early-phase panel of Fig. 2, we see that the model overestimate the data fluxes in the $\phi = -15$ to -10 d range. Figure 1 also show a flux excess in the $\phi = -18$ to -15 d period, especially in i and g . The SALT2 model does not prohibit the model flux from becoming negative, which are not physical. This is particularly true for low x_1 models. The early excess thus points towards a parameter modeling issue rather than a real physical effect.

In the $\phi = -15$ to -10 d period the model over-prediction suggests that the SN Ia lightcurve rise starts slightly later and rises slightly faster than what the model predicts. This is likely a regularization issue that penalizes fast evolution of the model era that have no sufficient training. At $\phi = -10$ d, the SALT2 model converges towards the correct SN Ia rise pace, likely thanks to sufficient training. This is visible in Fig. 2: the black line (model) clearly lies on top of the white marker (binned data).

4.1.2. Near max phases: $\phi \in [-5, +15]$ d.

It is remarkable to see so few deviations in Fig. 1 when applying the SALT2 model on our multi-thousand SN Ia dataset that never entered the model training. The near-max epoch range is indeed the one with the highest spectral and photometric training density, so it is not unexpected to observe that lightcurve residuals are globally flat and consistent with zero. Nonetheless, such an accuracy is reassuring for SN-cosmology as this particular phase-range, $\phi \in [-5, +15]$ d, is the most important for determining the SN lightcurve peak flux, stretch, and color from which distances are ultimately derived.

Yet, careful inspection of Fig. 1 reveals a small but significant flux excess in r . The model slightly under-estimates the observed flux the week of maximum light. Hence, either the SALT color-law (CL) is slightly off for this band ($\lambda \in [5650, 7250]$ Å) or the underlying spectral template model (M_0) is inaccurate in this phase range. This is further investigated in Sect. 4.3 where we analyse how lightcurve residuals vary as a function of lightcurve parameters.

4.1.3. Second bump phases: $\phi \in [+15, +35]$ d.

The second-peak period at $\phi \in [+15, +30]$ d corresponds to the arrival of heavy elements like Fe II in the explosion ejecta which, combined with a change of opacity, produces a flux increase in the red to near-infrared wavelengths (Kasen 2006). This period shows an interesting increase of the SN Ia luminosity, which should depend on progenitor and/or explosion mechanism properties (Dhawan et al. 2015). Yet, no particular lightcurve parameters have been defined in SALT for this period that could enable to reduce the SN Ia scatter in the Hubble diagram or reduce known astrophysical biases (see e.g. Folatelli et al. 2010; Papadogiannakis et al. 2019; Pessi et al. 2022, and reference therein).

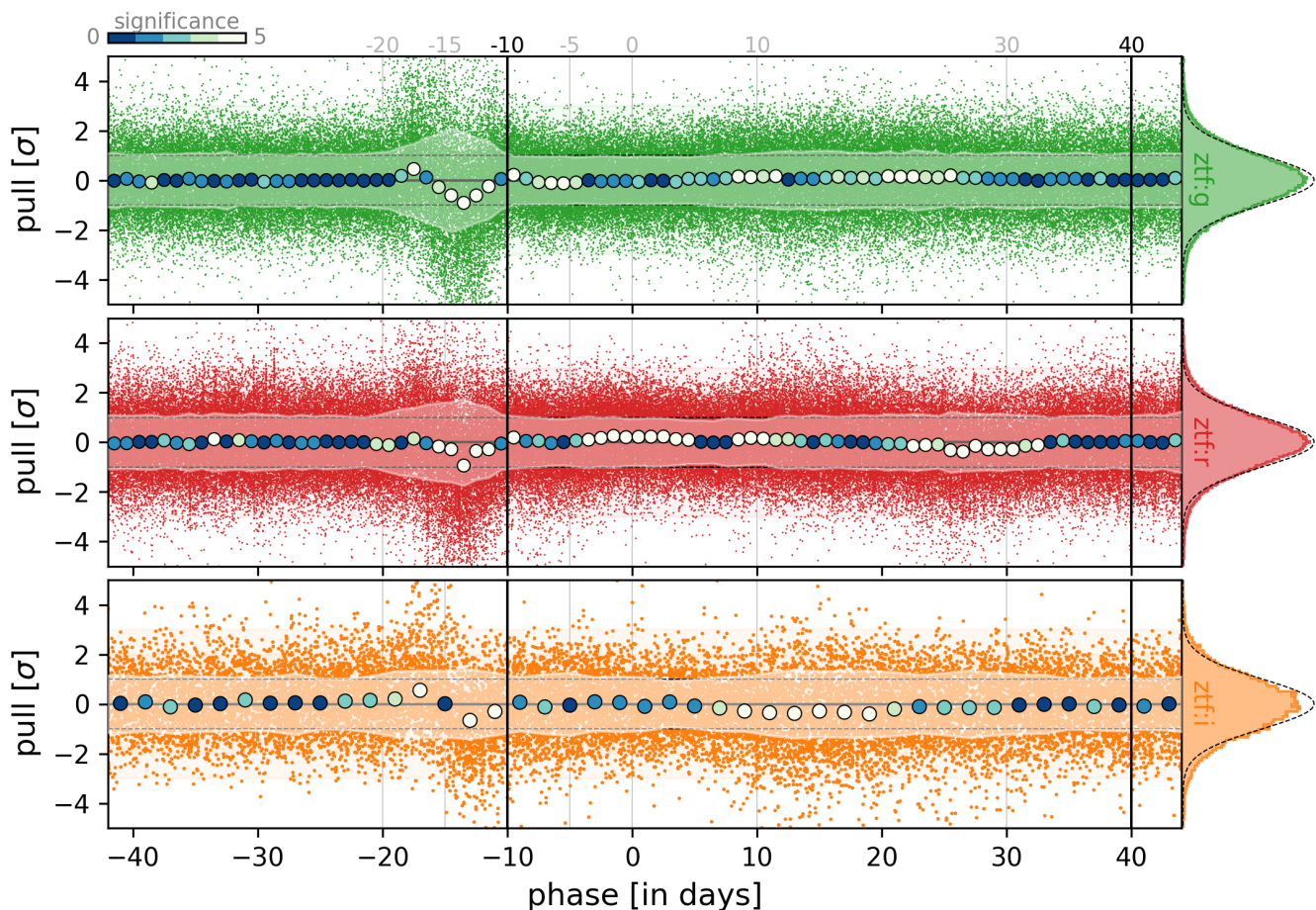


Fig. 1. Residual lightcurve fits in units of errors (i.e. the pull) as a function of rest-frame phase. From *top to bottom*: *g*- (green), *r*- (red) and *i*-bands (orange). The errors include the band-dependent error-floor, see Sect. 3. *In each panel*, small colored markers represent individual data-points (pull) while blue-to-white markers show the median pull per daily bin (2-d for *i* band). These markers are colored by the significance of their deviation from zero, white markers are non-zero at least at the 5σ level (see top-left “significance” color bar). The running white bands centered on zero show the bins nMAD. If the lightcurve model were to perfectly represent our data, and if our errors were Gaussian and correctly estimated, the pull should be centered on zero with a scatter of one. The thin dashed horizontal lines show the 1σ for reference. *Right-panel histograms* show the phase-marginalized distribution per band. A $\mathcal{N}(0, 1)$ distribution is also displayed as a thin dashed-line for reference. The black vertical lines show the phase range used to fit the lightcurve data $\phi \in [-10, +40]$ d. This figure contains 2625 SNe Ia.

Looking at Fig. 1, we see a small but long (nearly two weeks) model over-estimation of the flux in the *i* band. In the example shown in Fig. 2, we clearly see that the model is smoother than the data that show a stronger “elbow” at $\phi = +15$ d.

This smoothness issue is, again, likely due to a limited amount of rest-frame wavelength data redder than 7000 \AA since the SALT2 training sample is usually made of higher-redshift targets (Betoule et al. 2014; Taylor et al. 2021). For cosmology, the inability to correctly model the phase evolution of SN Ia lightcurves (the model is too smooth at $+15$ d, but also at -15 d, see Sect. 4.1.1) could lead to an inaccurate estimation of lightcurve parameters (x_0 , c and x_1), and then, in turn, to errors in the derivation of distances. A better “smoothness” modeling could thus improve the overall lightcurve fit. Furthermore, such an improvement on red- to near-infrared bands would help photo-typing methods as this second peak feature is unique to SNe Ia (e.g., Kasen 2006).

4.2. Study of the fitted phase-range

When fitting a lightcurve, one may want to include a phase range as large as possible to better constrain the model parameters.

That is especially true for the stretch. Yet, including ill-modelled phase ranges will bias the parameter estimations. For that reason, it is expected that phases outside the $\phi \in [-15, +45]$ d, that have nearly no training data (Betoule et al. 2014; Taylor et al. 2021; Kenworthy et al. 2021), should not be included.

Figure 3 shows the lightcurve residuals when lightcurves are fitted using the $\phi \in [-5, +30]$ d phase range. We see very similar structure as in Fig. 1, showing that the inclusion of $\phi \in [-10, -5]$ d and $\phi \in [+30, +40]$ d phases does not bias the lightcurve modeling: SN Ia lightcurves are well modeled in the extrapolated $\phi = [-10, -5]$ and $[+30, +40]$ d phase ranges since residuals are consistent with 0 in all three ZTF bands.

Hence, to get the most accurate and precise lightcurve fits, we consider the wider well modeled phase-range for the ZTF-Cosmo-DR2 fits and we thus advocate to use $\phi = [-10, +40]$ d and this is consequently the rest-frame phase range used for the “DR2” release (Rigault et al. (a), Smith et al.).

4.3. As a function of lightcurve parameters

We present in Fig. 4 and Fig. 5 the lightcurve residuals when splitting our SN Ia sample by their lightcurve color (c) and

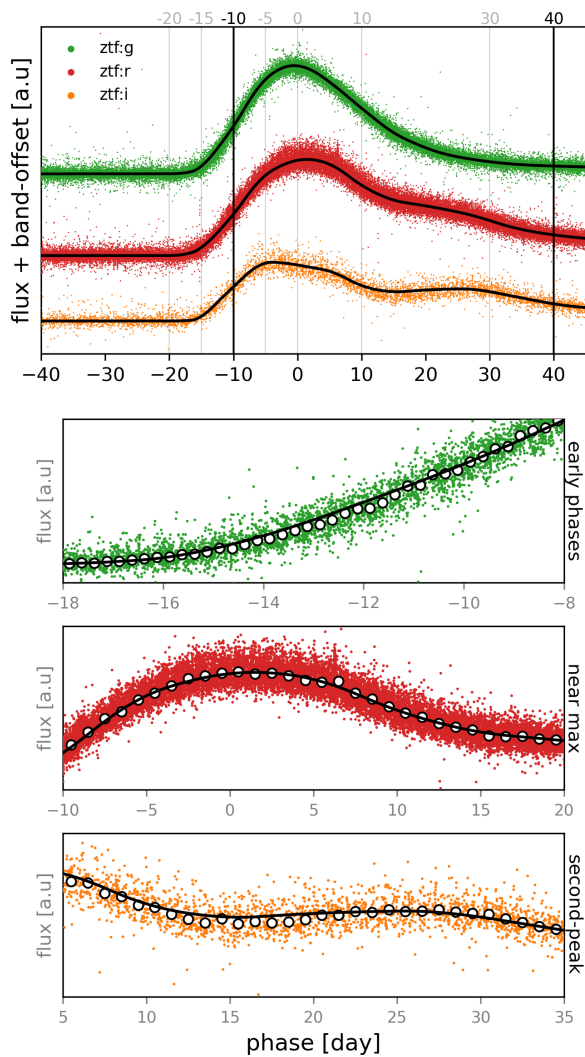


Fig. 2. Example of Type Ia supernova lightcurves normalized by their SALT2 flux intensity parameter x_0 . For this illustration, only targets passing the following criteria have been displayed (see Sect. 4.1): $z \in [0.05, 0.09]$; $c \in [-0.1, 0.1]$ and $x_1 \in [-1, 1]$. In each panel, the black lines represent the SALT2 model at the median redshift ($z = 0.07$), color ($c = 0.01$) and stretch ($x_1 = 0.17$). *Bottom panels:* zoom on specific time periods illustrated by a given band; *from top-to-bottom:* early phases (g), near maximum light (r) and the second peak period (i). White markers show daily bin median fluxes (quarter of a day for the early phases). This figure contains 781 SNe Ia.

stretch (x_1), respectively. Doing so enables us to investigate the potential origin of observed deviations. For instance, residual variations observed regardless of the lightcurve parameters would point toward issues in the average template $M_0(\phi, \lambda)$, while color-dependent but phase-independent residuals would point toward a mis-calibration of the SALT2 color-law $CL(\lambda)$. However, we highlight that SN lightcurve features not captured by the SALT2 model would likely lead to residual variation scatter across the entire lightcurve phase range. It is then by splitting the SNe along a parameter that could be related to the missing part of the model (e.g. observed host biases) that one may unveil such an effect.

We investigate the color-dependencies (Fig. 4, Sect. 4.3.1) first, and the stretch-dependencies (Fig. 5, Sect. 4.3.2) second. The host-dependencies are presented in Sect. 4.4.

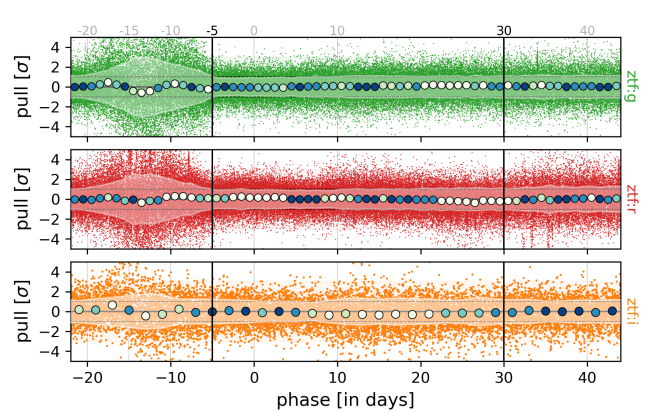


Fig. 3. Similar to Fig. 1, but with a fitted phase range $\phi \in [-5, +30]$ d; see black vertical lines.

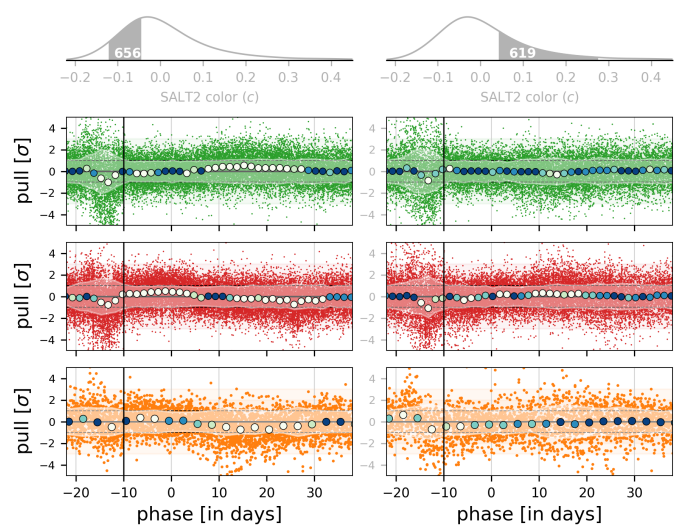


Fig. 4. Similar to Fig. 1, but split per lightcurve color (c) to separately probe blue and red SNe Ia. For visibility, phase bins are 1.5 d in g and 3 d in i . *Left side:* $c \in [5\%, 30\%]$ percentiles SNe Ia; *Right side:* $c \in [70\%, 95\%]$ percentiles SNe Ia. *Top:* SN Ia color distributions highlighting the part considered on each side, indicating the corresponding sample size.

4.3.1. Color-dependency

The SN Ia color is thought to be a mixed contribution between intrinsic color variations (dominating at $c < 0$) and external extinction caused by host-interstellar dust (dominating at $c > 0.2$; see e.g., Brout & Scolnic 2021; Popovic et al. 2021 and references therein). Figure 4 shows the lightcurve residuals of bluer and redder SNe Ia, separately. Surprisingly, redder SNe Ia ($c \in [0.05, 0.28]$, the 70%-95% c -range) appear globally better modeled by SALT than bluer ones ($c \in [-0.11, -0.03]$, 5%-30%) as they have less significant deviations. It is surprising since the SN Ia lightcurve modeling more strongly depends on the $CL(\lambda)$ when $|c|$ is high. Conversely, $CL(\lambda)$ has no effect for a $c = 0$ target.

When looking in detail at the blue SNe Ia in Fig. 4, we notice that before maximum light, r - and i -band lightcurves are underestimated (negative pull) while g -band light-curves are overestimated. This inverts at phase $\phi = +10$ d and converges towards

zeros only by phase $\phi = +30$ d. We do not see such behavior for redder targets.

One has to remember that the SALT color-law $CL(\lambda)$ is phase independent and the first template order, $M_0(\phi, \lambda)$, does not depend on any lightcurve parameters. In other words: red and blue SNe Ia lightcurves are modeled by the same $M_0(\phi, \lambda)$ and deformed by $c \times CL(\lambda)$, and this deformation is phase-independent. It is thus intriguing to observe SN-color *and* phase dependent residual variations. In principle, stretch and color corrections are independent. Yet, to ensure that what we report is not affected by x_1 -related issue we did the same analysis considering $x_1 \in [-0.5, +1.5]$ or $x_1 \in [-2.0, -0.5]$ SNe Ia only. Doing so, we found the exact same results when comparing blue and red SNe Ia. Hence, the phase-dependent features visible in Fig. 4 are not related to potential $M_1(\phi, \lambda)$ template issues.

It is consequently very likely that an extension to the SALT2 model is required to capture the observed phase- and color-dependent variations. As a physical interpretation, the current phase-independent $CL(\lambda)$ would capture external dust absorption, while the additional $CL_{\text{int}}(\phi, \lambda)$ would account for potential intrinsic SN color variations. This would be in line with recent findings about multiple SN color origins (e.g. Brout & Scolnic 2021; Nascimento et al. 2023; Hand in prep.) Kenworthy et al. extends the SALT3 model to include an additional parameter, which captures this additional phase-dependence of SN Ia colors, in agreement with this work.

4.3.2. Stretch-dependency

The SN Ia stretch is an intrinsic property directly connected to the astrophysics of the SN Ia explosion event (e.g., Scalzo et al. 2014; Shen et al. 2021, and reference therein). It has been shown to depend on the SN Ia environment, and most likely on the progenitor age (e.g. Hamuy et al. 1996; Howell et al. 2007; Nicolas et al. 2021). Lightcurve deviations as a function of SN Ia stretch could provide interesting clues to further understand SN Ia physics and help constrain observed astrophysical biases in SN cosmology.

Figure 5 shows the SALT2 lightcurve residuals for fast ($x_1 \in [-2.2, -0.1]$) and slow-declining SNe Ia ($x_1 \in [+0, +1]$), separately (bins selected to sample the two stretch modes, see e.g., Nicolas et al. 2021). The lightcurve residuals appear globally flat, suggesting that the stretch template correction ($M_1(\phi, \lambda)$) seems to quantitatively well describe the data. This is particularly true for the high-stretch mode, the most populated. For these supernovae, the sole significant deviation is in the i -band and is consistent with the effect already discussed in Sect. 4 and visible in Fig. 1 and in Fig. 2: i.e. the SALT2 template is smoother than the data. Low-stretch mode SNe Ia, however, show some significant deviations in the r -band. The phase range near the second-peak ($\phi \sim +25$ d) is particularly affected suggesting that the $M_1(\phi, \lambda)$ structure itself would benefit for a retraining, and not just the SALT2 regularization terms. At maximum light, deviations are likely collateral issues caused by the late phase issue. The g and i -bands are nonetheless correctly modelled, suggesting that this r -band issue does not significantly affect the overall fit. Overall, with the current SALT2 template, high-stretch mode SNe Ia are better modelled than low-stretch ones. This issue is likely due to the linear construction of the SALT model; non-linear models such as ParSNIP (Boone 2021) and SNooPy (Burns et al. 2011) are inherently more capable of simultaneously modeling both the extremes and the middle of the stretch distribution than SALT. Resolving the issue will re-

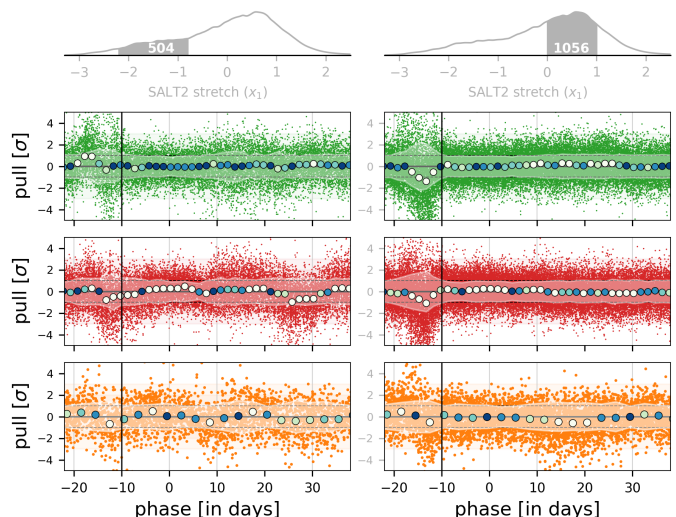


Fig. 5. Similar to Fig. 1, but split per lightcurve stretch (x_1) to sample both modes (Nicolas et al. 2021, Ginolin et al.). For visibility, phase bins are of 1.5 d in g and r and 3 d in i . *Left side:* $x_1 \in [-2.2, -0.8]$ SNe Ia ; *Right side:* $x_1 \in [0, +1.0]$ SNe Ia. *Top:* SN Ia stretch distributions highlighting the sample considered on each side.

quire adding some degree of non-linearity to the model, or over-compensating with additional linear parameters.

Finally, the strong bump visible at low-stretch in the g -band is a consequence of the negative-flux modeling in SALT2 that has already been discussed in Sect. 4 and is not connected to the SN Ia physics.

4.4. As a function of host environment

In this subsection we investigate how SN Ia lightcurve residuals vary as a function of their environment. Deviations are expected since SN Ia parameters and, most importantly, standardized SN Ia magnitudes have been shown to significantly depend on their host environments (see e.g., Sullivan et al. 2010; Roman et al. 2018; Rigault et al. 2020; Briday et al. 2022 and companion ZTF-Cosmo-DR2 paper Ginolin et al.). The community is looking for an additional lightcurve parameter which could capture such dependencies.

Following most of literature analyses we focus here on the global host stellar-mass ($\log(M_*/M_\odot)$) and the local environment color tracer ($(g-z)_{\text{local}}$; see parameter estimation in Rigault et al. (a) and Smith et al.). The lightcurve residuals as a function of their environments are shown in Fig. 6. Surprisingly, we see no significant host-signature in the lightcurve residuals. Low- and high-mass host SNe Ia have very similar residuals, as do locally blue- and red-environment targets. The only noticeable change is seen in the i -band at the time of the second peak, but this very likely connected to the similar differences as a function of the SN lightcurve stretch, since low-stretch mode SNe Ia only exist in massive host and/or red environments (see e.g. Nicolas et al. 2021 and Ginolin et al.). This is in agreement with the results of Jones et al. (2023), which found limited evidence for photometric variation in SN Ia explainable with host-galaxy properties.

We therefore conclude that it is unlikely that lightcurve parameter could capture SN-host dependencies, at least not in the optical photometric bands ZTF probes. This conclusion might

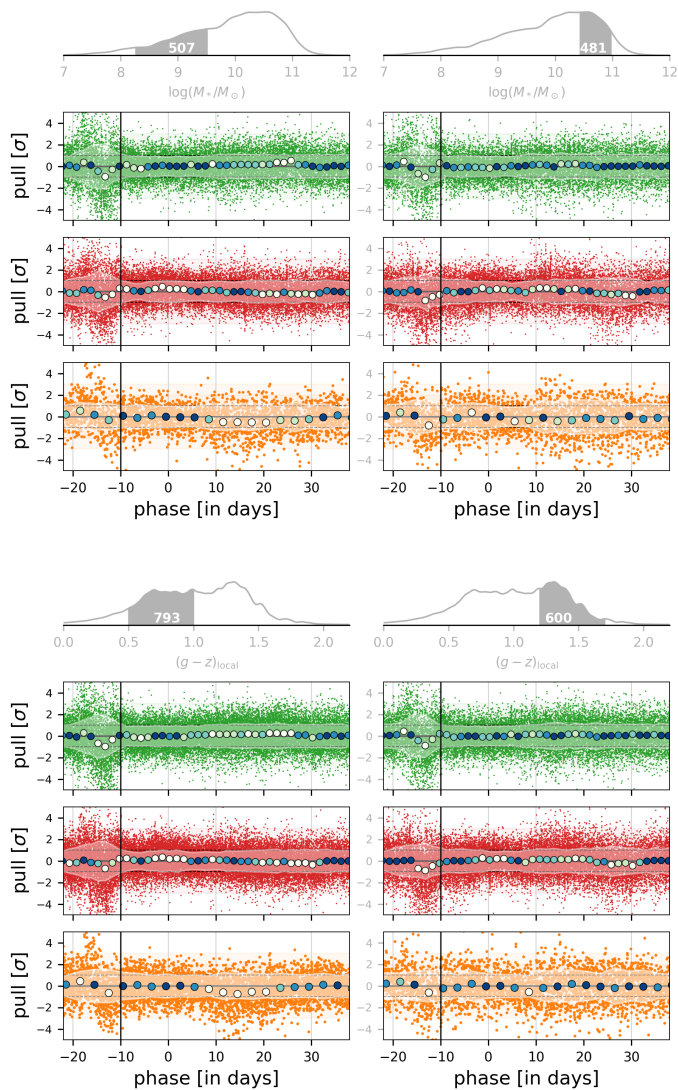


Fig. 6. Similar to Fig. 5 and 4, but split per global host mass ($\log(M_*/M_\odot)$, *top*) or by local color environment ($(g-z)_{\text{local}}$, *bottom*).

be revisited once the color- and phase-dependent variations presented in Sect. 4.3.1 are accounted for.

4.5. SALT2 vs. SALT3

In the main analysis we use the SALT2 (Guy et al. 2010) algorithm trained by Taylor et al. (2021), extending the original 2.4 version from Betoule et al. (2014). Recently, Kenworthy et al. (2021) re-design the training algorithm and created SALT3. In this section we investigate whether our results hold if we were to use this SALT implementation.

The SALT3 lightcurve fit residuals are shown in Fig. 7. Deviations observed with SALT2 visible Fig. 1 and discussed in Sect. 3 are still visible, some even stronger:

1. early phases $[-20, -10]$ d fluxes are strongly overestimated by the lightcurve fitter in all three bands.
2. the model is largely under-estimating the r -band flux near peak brightness ($[-5, +5]$ d)
3. the second peak epoch ($[+15, +35]$ d) still shows deviations, but they appear weaker in SALT3 than in SALT2 unlike the two other issues that are stronger in SALT3.

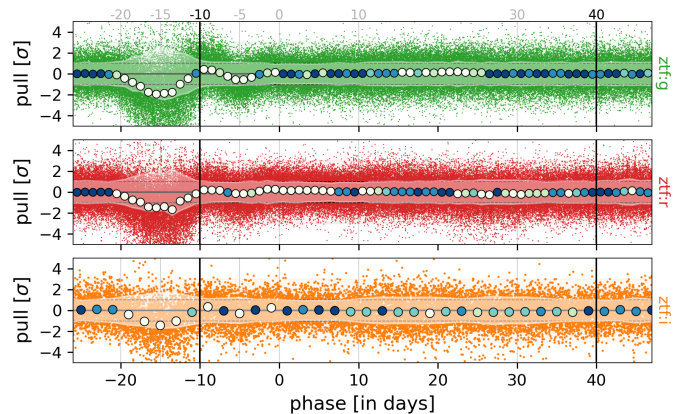


Fig. 7. Similar as Fig. 1, but using the SALT3 lightcurve fitting algorithm (Kenworthy et al. 2021). Variations observed with SALT2 are still visible, notably pre-max where they are even stronger.

In addition, there is a strong deviation at -5 d in SALT3 that does not seem significant in SALT2 ; especially in the g band.

When investigating the aforementioned variations when splitting SNe Ia by stretch (Sect. 4.3.2) or color (Sect. 4.3.1), we see very similar features and draw the same conclusions as we did when using SALT2. We thus conclude that SALT3 is very similar to SALT2 in describing the ZTF lightcurve data. SALT3 seems slightly better at describing the second-peak epoch but does significantly worse pre-maximum light, indicating that future trainings should reduce the degree of regularization applied. Altogether, we encourage to wait for a future SALT3 version prior using it for precision cosmology, though the current implementation has been shown to resolve other issues relevant to cosmology as compared to SALT2 (see details in Taylor et al. 2023). We used version 2.0, as available in snocosmo.

5. Lightcurve parameter variations

In this section, we investigate how the ZTF-Cosmo-DR2 SALT2 parameters depend on choices to perform the lightcurve fit, i.e. using the $\phi \in [-10, +40]$ d phase range and using all three ZTF bands when available. In Sect. 5.1 we discuss phase variations, and in Sect. 5.2 we investigate if the presence of the i band has significant impact on the derivation of the SALT2 lightcurve parameters.

5.1. Impact of different fitted phase range

We compare the estimation of the SALT2 lightcurve parameters when changing the reference $\phi \in [-10, +40]$ d phase range to either the smaller $\phi \in [-5, +30]$ d one, or one with a longer baseline $\phi \in [-20, +50]$ d. The $\phi \in [-10, +40]$ d vs. $\phi \in [-5, +30]$ d phase range comparison is shown in Fig. 8.

In that figure, we see that the SALT2 parameters seem unbiased when reducing the covered phase range. The scatter on x_1 , the most sensible parameter to phase coverage, is of the order of the typical x_1 error (~ 0.2). The SALT2 color (c) or peak magnitude (derived from x_0) variations are typically smaller than 30% of the quoted errors. When the default phase-range is compared to the $\phi \in [-20, +50]$ d phase range instead of the shorter $\phi \in [-5, +30]$ d (not shown) the conclusions are the same, but with variations typically half of that presented in Fig. 8.

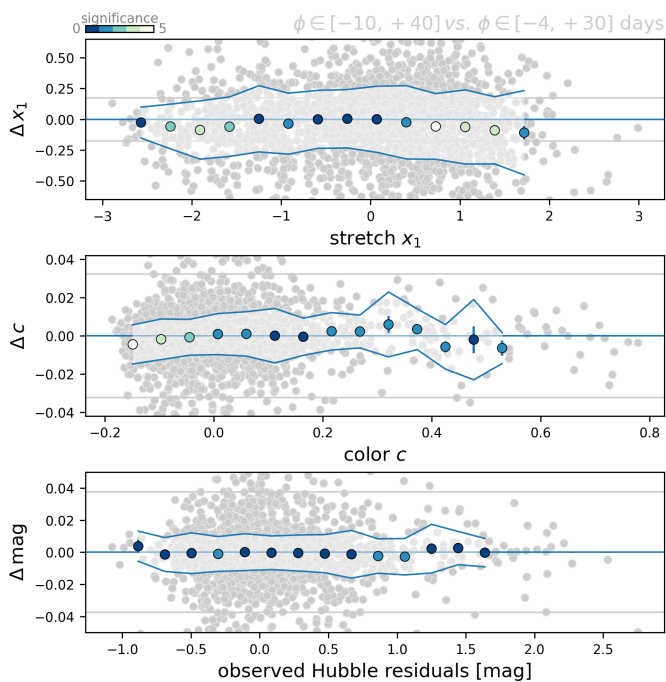


Fig. 8. Impact of changing the fitted phase range from $\phi \in [-10, +40]$ (“*ref*”) to $\phi \in [-5, +30]$ (“*comp*”) on estimating the SALT2 lightcurve parameters x_1 (*top*), c (*middle*), and observed Hubble residuals, derived from x_0 assuming a default cosmology (*bottom*). The x-axis in each panel shows the reference parameter (e.g. c_{ref}), while the y-axis is the difference ($\Delta c \equiv c_{ref} - c_{comp}$). In each panel, the horizontal grey line show the median parameter error and the marker color indicates the significance of the deviation from zero.

We thus conclude that our SN lightcurve parameter estimations are robust against reasonable changes in the fitted phase range. This robustness is largely due to the impressive ZTF cadence (typically one photometric point per day, see [Rigault et al.](#)).

5.2. Missing the *i* band

We now investigate the impact of the use (or not) of the *i*-band data when estimating the lightcurve parameters. As reported in [Rigault et al.](#) and [Smith et al.](#), only 46% of our targets have at least one *i*-band detection within the $\phi \in [-10, +40]$ d phase-range. Only 25% have at least 5 detections. This questions the self-consistency of the SALT2 lightcurve parameters estimation between SNe Ia with and those without *i*-band coverage.

To test this, we compare the SALT2 parameters estimated with and without *i* band by refitting the lightcurve parameters while discarding our *i*-band data. The resulting SALT2 color variations, the most impacted parameter by far, and the resulting *i*-band lightcurve residuals are shown in [Fig. 9](#). In that figure, we see that the SALT2 colors vary by less than 0.01, less than a third of the typical SALT2 color parameter errors. This demonstrates that the SALT2 parameters estimated for targets with or without *i*-band data are compatible. This is further supported by the *i*-band lightcurve residuals presented in [Fig. 9](#). The residual scatters are centered on zero and do not show more biases than these already presented in this paper. The only noticeable variation is the slight scatter increase (running white band). This is to be expected since the *i*-band lightcurve never entered the fit, and the shown residuals are the result of an extrapolation of the *g*, *r* fitted SALT2 model to the *i*-band. In fact, such remarkable

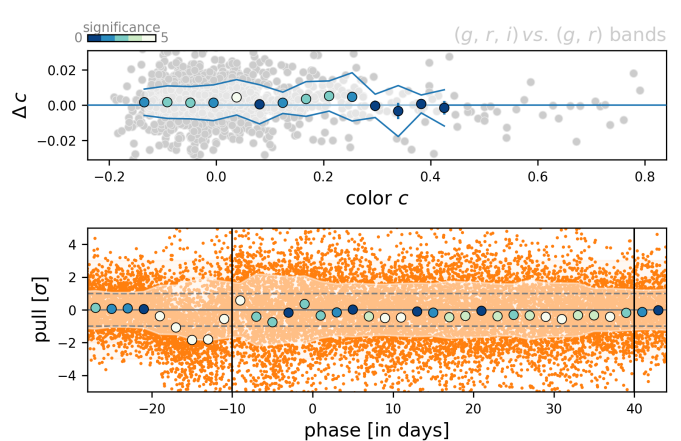


Fig. 9. Impact on using *g*- and *r*-bands only to fit ZTF lightcurve data with SALT2. *Top* variation of the color c parameter, cases with no *i*-band data (55%) are shown in grey. *Bottom* *i*-band lightcurve fit residuals (not used for the fit) shown following [Fig. 1](#)'s layout.

agreement of the *i*-band lightcurve residuals strengthen the quality of the ZTF-Cosmo-DR2 band inter-calibration.

In light of the results presented in this subsection, one could question the interest of acquiring *i*-band data for SN cosmology. Here, we thus briefly summarize a few points.

Let us first remind that this study is made in the context of the SALT2 algorithm that only has one color parameter. Two bands are thus sufficient, in principle, and since the ZTF, *g*- and *r*-band observations are 4 times more frequent than the *i*-band observations (~ 1.5 d vs. ~ 5 d cadence) and are deeper (20.5 mag vs. 20 mag, [Smith et al.](#)), they largely overweight the *i*-band information during the SALT2 lightcurve fit. But the *i*-band is important in SN cosmology for at least three reasons.

Calibration first: three bands enable to diagnose any calibration systematic within the bands as we can use two to predict the third. Astrophysics second: the existence of two colors in SN Ia standardization is highly debated (e.g. [Brout & Scolnic 2021](#), and reference therein). Three bands are thus needed to confirm or not the existence of two color term in SN cosmology. And, if indeed confirmed, the *i*-band will be required to derive accurate distances (see also [Sect. 4.3](#)). Operational third: red to near-infrared regions are where SNe Ia differ the most from other SN types. The *i*-band is thus powerful to discriminate a SN Ia from another kind of transient.

SN cosmological surveys then need to acquire data in at least 3 bands.

6. Conclusion

This paper presents a detailed study of the ZTF “DR2” SN Ia lightcurve residuals with respect to the SALT2 model. We study the accuracy of the model, that we did not retrain, to fit our *g*-, *r*- and *i*-band dataset made of 2625 SNe Ia. In particular, we investigate: (1) which phase-range should be considered for the lightcurve fit ; (2) the impact of missing the *i*-band data for 55% of our targets for the estimation of their lightcurve parameters ; (3) if the SALT2 model equally well describes SN Ia lightcurves regardless of their parameter or host environments. Such a study matters for SN cosmology since the use of the SALT2 lightcurve fitter is a core ingredient for the derivation of distances. Inaccuracy of the model to explain the data could then lead to biases in the derivation of cosmological parameters.

Our conclusions are the following:

1. Globally, the current implementation of SALT2 (2.4 or T21) remarkably well represents our dataset, even though our sample is much larger than that used for the model training. In all three optical ZTF bands, the model residuals from rest-frame phases ϕ between -10 to $+40$ d systematically deviate from zero only a tenth of the errors.
2. The lightcurve flux error estimations of the ZTF-Cosmo-DR2 are compatible with the observed data once including a 2.5%, 3.5% and 6% SN flux scatter to account for noise introduced by the difference image pipeline. The amplitude of this error-floor is compatible with findings based on simulations reported in the companion paper (Amenouche et al.).
3. The SALT2 model is not able to describe the early SN Ia lightcurve phases ($\phi < -10$ d), when it systematically overestimate the observed flux. This is particularly true for g and r bands. This issue is most likely due to a lack of training data in that phase range and should be fixed by including datasets like ZTF in the training set.
4. When comparing the SNe Ia per host environment we see no sign a lightcurve residual differences. This strongly suggests that the SN optical lightcurves do not contain a signature that would enable us to absorb the observed environmental dependencies in SN standardized magnitude (aka “the steps”). Improved early epoch modeling and color (see below) may change this conclusion.
5. We show many small but significant biases (non-zero residuals) in many epochs of the lightcurves, even in the $\phi \in [-10, +40]$ d phase-range. Most notably, at maximum light the r -band flux is under-estimated and many deviations are visible around the second peak in all three bands. The SALT2 model seems globally too smooth in fine in comparison to what the data would favor. It is very likely that a retraining of the SALT2 model with additional data would absorb these variations.
6. We report significant lightcurve residual variations for blue and red SNe Ia that seem unlikely to be absorbed by a retraining the SALT2 model. They rather strongly suggest the existence of a third component in the form of a phase-dependent color term. Its impact of the overall lightcurve modeling might be small, but its estimation could reveal important for cosmology since claims of multiple sources of SN color are often made.
7. Lightcurve variations are stronger in low-stretch SNe Ia, which is again not surprising as these are rarer and fainter and are thus not so represented in the training dataset.
8. The SALT2 parameters reported in the ZTF-Cosmo-DR2 are robust against phase variations ($\phi \in [-5, +30]$ or $\phi \in [-20, +50]$ d in place of the default $\phi \in [-10, +40]$ d) or against the existence or not of i -band data.
9. SALT3, with its version 2.0, show significantly more lightcurve residual deviations than SALT2 (T21 or 2.4-JLA), and should then not be favored for precision cosmology prior updates fixing these issues.

In light of this paper, we strongly advocate that SN cosmological analyses should include a retraining of the lightcurve fitter model to accurately represent the complexity of the considered dataset. That is critical for samples significantly larger than that used to train the model. Consequently, cosmological analyses based in ZTF data will require a retraining of the SALT model. We finally encourage modellers to consider looking for a color-dependent term that could explain the observed color-dependency variations of the lightcurve residuals. This might reveal important for SN cosmology.

Acknowledgements. Based on observations obtained with the Samuel Oschin Telescope 48-inch and the 60-inch Telescope at the Palomar Observatory as part of the Zwicky Transient Facility project. ZTF is supported by the National Science Foundation under Grants No. AST-1440341 and AST-2034437 and a collaboration including current partners Caltech, IPAC, the Weizmann Institute of Science, the Oskar Klein Center at Stockholm University, the University of Maryland, Deutsches Elektronen-Synchrotron and Humboldt University, the TANGO Consortium of Taiwan, the University of Wisconsin at Milwaukee, Trinity College Dublin, Lawrence Livermore National Laboratories, IN2P3, University of Warwick, Ruhr University Bochum, Northwestern University and former partners the University of Washington, Los Alamos National Laboratories, and Lawrence Berkeley National Laboratories. Operations are conducted by COO, IPAC, and UW. SED Machine is based upon work supported by the National Science Foundation under Grant No. 1106171 The ZTF forced-photometry service was funded under the Heising-Simons Foundation grant #12540303 (PI: Graham). This project has received funding from the European Research Council (ERC) under the European Union’s Horizon 2020 research and innovation program (grant agreement n 759194 - USNAC). This project is supported by the H2020 European Research Council grant no. 758638. This work has been supported by the Agence Nationale de la Recherche of the French government through the program ANR-21-CE31-0016-03. L.G. acknowledges financial support from the Spanish Ministerio de Ciencia e Innovación (MCIN) and the Agencia Estatal de Investigación (AEI) 10.13039/501100011033 under the PID2020-115253GA-I00 HOSTFLOWS project, from Centro Superior de Investigaciones Científicas (CSIC) under the PIE project 20215AT016 and the program Unidad de Excelencia María de Maeztu CEX2020-001058-M, and from the Departament de Recerca i Universitats de la Generalitat de Catalunya through the 2021-SGR-01270 grant. Y.-L.K. has received funding from the Science and Technology Facilities Council [grant number ST/V000713/1]. This work has been enabled by support from the research project grant ‘Understanding the Dynamic Universe’ funded by the Knut and Alice Wallenberg Foundation under Dnr KAW 2018.0067. SD acknowledges support from the Marie Curie Individual Fellowship under grant ID 890695 and a Junior Research Fellowship at Lucy Cavendish College. We thank the Heising-Simons Foundation for supporting the research program of SRK.

References

- Aldering, G., Adam, G., Antilogus, P., et al. 2002, *Proc. SPIE*, 4836, 61. doi:10.1117/12.458107
- Barbary et al. 2023, Zenodo. doi: 10.5281/zenodo.8393360.
- Bellm, E. C., Kulkarni, S. R., Graham, M. J., et al. 2019, *PASP*, 131, 018002. doi:10.1088/1538-3873/aaecbe
- Betoule, M., Kessler, R., Guy, J., et al. 2014, *A&A*, 568, A22. doi:10.1051/0004-6361/201423413
- Boone, K., Aldering, G., Antilogus, P., et al. 2021, *ApJ*, 912, 70. doi:10.3847/1538-4357/abec3c
- Boone, K., Aldering, G., Antilogus, P., et al. 2021, *ApJ*, 912, 71. doi:10.3847/1538-4357/abec3b
- Boone, K. 2021, *AJ*, 162, 275. doi:10.3847/1538-3881/ac2a2d
- Briday, M., Rigault, M., Graziani, R., et al. 2022, *A&A*, 657, A22. doi:10.1051/0004-6361/202141160
- Brout, D. & Scolnic, D. 2021, *ApJ*, 909, 26. doi:10.3847/1538-4357/abd69b
- Brout, D., Scolnic, D., Popovic, B., et al. 2022, *ApJ*, 938, 110. doi:10.3847/1538-4357/ac8e04
- Burns, C. R., Stritzinger, M., Phillips, M. M., et al. 2011, *AJ*, 141, 19. doi:10.1088/0004-6256/141/1/19
- Dhawan, S., Leibundgut, B., Spyromilio, J., et al. 2015, *MNRAS*, 448, 1345. doi:10.1093/mnras/stu2716
- Dimitriadis, G., Foley, R. J., Rest, A., et al. 2019, *ApJ*, 870, L1. doi:10.3847/2041-8213/aaedb0
- Deckers, M., Maguire, K., Magee, M. R., et al. 2022, *MNRAS*, 512, 1317. doi:10.1093/mnras/stac558
- Deckers, M., Graur, O., Maguire, K., et al. 2023, *MNRAS*, 521, 4414. doi:10.1093/mnras/stad841
- Fakhouri, H. K., Boone, K., Aldering, G., et al. 2015, *ApJ*, 815, 58. doi:10.1088/0004-637X/815/1/58
- Firth, R. E., Sullivan, M., Gal-Yam, A., et al. 2015, *MNRAS*, 446, 3895. doi:10.1093/mnras/stu2314
- Folatelli, G., Phillips, M. M., Burns, C. R., et al. 2010, *AJ*, 139, 120. doi:10.1088/0004-6256/139/1/120
- Freedman, W. L., Madore, B. F., Hatt, D., et al. 2019, *ApJ*, 882, 34. doi:10.3847/1538-4357/ab2f73
- Goobar, A. & Leibundgut, B. 2011, *Annual Review of Nuclear and Particle Science*, 61, 251. doi:10.1146/annurev-nucl-102010-130434
- Grayling, M., Thorp, S., Mandel, K. S., et al. 2024, arXiv:2401.08755. doi:10.48550/arXiv.2401.08755

- Graham, M. J., Kulkarni, S. R., Bellm, E. C., et al. 2019, *PASP*, 131, 078001. doi:10.1088/1538-3873/ab006c
- Guy, J., Astier, P., Baumont, S., et al. 2007, *A&A*, 466, 11. doi:10.1051/0004-6361:20066930
- Guy, J., Sullivan, M., Conley, A., et al. 2010, *A&A*, 523, A7. doi:10.1051/0004-6361/201014468
- Hamuy, M., Phillips, M. M., Suntzeff, N. B., et al. 1996, *AJ*, 112, 2438. doi:10.1086/118193
- Howell, D. A., Sullivan, M., Conley, A., et al. 2007, *ApJ*, 667, L37. doi:10.1086/522030
- Jha, S., Riess, A. G., & Kirshner, R. P. 2007, *ApJ*, 659, 122. doi:10.1086/512054
- Jones, D. O., Kenworthy, W. D., Dai, M., et al. 2023, *ApJ*, 951, 22. doi:10.3847/1538-4357/acd195
- Kasen, D. 2006, *ApJ*, 649, 939. doi:10.1086/506588
- Kelly, P. L., Hicken, M., Burke, D. L., et al. 2010, *ApJ*, 715, 743. doi:10.1088/0004-637X/715/2/743
- Kelsey, L., Sullivan, M., Wiseman, P., et al. 2023, *MNRAS*, 519, 3046. doi:10.1093/mnras/stac3711
- Kenworthy, W. D., Jones, D. O., Dai, M., et al. 2021, *ApJ*, 923, 265. doi:10.3847/1538-4357/ac30d8
- Léget, P.-F., Gangler, E., Mondon, F., et al. 2020, *A&A*, 636, A46. doi:10.1051/0004-6361/201834954
- Mandel, K. S., Thorp, S., Narayan, G., et al. 2022, *MNRAS*, 510, 3939. doi:10.1093/mnras/stab3496
- Müller-Bravo, T. E., Sullivan, M., Smith, M., et al. 2022, *MNRAS*, 512, 3266. doi:10.1093/mnras/stab3065
- Nascimento, C. S., França, P. C., & Reis, R. R. R. 2023, arXiv:2310.02329. doi:10.48550/arXiv.2310.02329
- Nicolas, N., Rigault, M., Copin, Y., et al. 2021, *A&A*, 649, A74. doi:10.1051/0004-6361/202038447
- Papadogiannakis, S., Goobar, A., Amanullah, R., et al. 2019, *MNRAS*, 483, 5045. doi:10.1093/mnras/sty3301
- Perlmutter, S., Aldering, G., Goldhaber, G., et al. 1999, *ApJ*, 517, 565. doi:10.1086/307221
- Pessi, P. J., Hsiao, E. Y., Folatelli, G., et al. 2022, *MNRAS*, 510, 4929. doi:10.1093/mnras/stab3593
- Phillips, M. M. 1993, *ApJ*, 413, L105. doi:10.1086/186970
- Planck Collaboration, Aghanim, N., Akrami, Y., et al. 2020, *A&A*, 641, A6. doi:10.1051/0004-6361/201833910
- Popovic, B., Brout, D., Kessler, R., et al. 2021, arXiv:2112.04456. doi:10.48550/arXiv.2112.04456
- Roman, M., Hardin, D., Betoule, M., et al. 2018, *A&A*, 615, A68. doi:10.1051/0004-6361/201731425
- Rose, B. M., Baltay, C., Hounsell, R., et al. 2021, arXiv:2111.03081. doi:10.48550/arXiv.2111.03081
- Riess, A. G., Press, W. H., & Kirshner, R. P. 1996, *ApJ*, 473, 88. doi:10.1086/178129
- Riess, A. G., Filippenko, A. V., Challis, P., et al. 1998, *AJ*, 116, 1009. doi:10.1086/300499
- Riess, A. G., Yuan, W., Macri, L. M., et al. 2022, *ApJ*, 934, L7. doi:10.3847/2041-8213/ac5c5b
- Rigault, M., Copin, Y., Aldering, G., et al. 2013, *A&A*, 560, A66. doi:10.1051/0004-6361/201322104
- Rigault, M., Aldering, G., Kowalski, M., et al. 2015, *ApJ*, 802, 20. doi:10.1088/0004-637X/802/1/20
- Rigault, M., Brinnel, V., Aldering, G., et al. 2020, *A&A*, 644, A176. doi:10.1051/0004-6361/201730404
- Rubin, D., Aldering, G., Astraatmadja, T. L., et al. 2022, arXiv:2206.10632. doi:10.48550/arXiv.2206.10632
- Saunders, C., Aldering, G., Antilogus, P., et al. 2018, *ApJ*, 869, 167. doi:10.3847/1538-4357/aaec7e
- Scalzo, R., Aldering, G., Antilogus, P., et al. 2014, *MNRAS*, 440, 1498. doi:10.1093/mnras/stu350
- Schlafly, E. F., Finkbeiner, D. P. 2011, *ApJ*, 737, 103. doi:10.1088/0004-637X/737/2/103
- Scolnic, D. M., Jones, D. O., Rest, A., et al. 2018, *ApJ*, 859, 101. doi:10.3847/1538-4357/aab9bb
- Shen, K. J., Blondin, S., Kasen, D., et al. 2021, *ApJ*, 909, L18. doi:10.3847/2041-8213/abe69b
- Sullivan, M., Conley, A., Howell, D. A., et al. 2010, *MNRAS*, 406, 782. doi:10.1111/j.1365-2966.2010.16731.x
- Taylor, G., Lidman, C., Tucker, B. E., et al. 2021, *MNRAS*, 504, 4111. doi:10.1093/mnras/stab962
- Taylor, G., Jones, D. O., Popovic, B., et al. 2023, *MNRAS*, 520, 5209. doi:10.1093/mnras/stad320
- Tripp, R. 1998, *A&A*, 331, 815
- Wiseman, P., Vincenzi, M., Sullivan, M., et al. 2022, *MNRAS*, 515, 4587. doi:10.1093/mnras/stac1984
-
- ¹ Université Claude Bernard Lyon 1, CNRS, IP2I Lyon / IN2P3, IMR 5822, F-69622 Villeurbanne, France
- ² Department of Physics, Lancaster University, Lancs LA1 4YB, UK
- ³ Sorbonne Université, CNRS/IN2P3, LPNHE, F-75005, Paris, France
- ⁴ The Oskar Klein Centre, Department of Physics, AlbaNova, SE-106 91 Stockholm, Sweden
- ⁵ School of Physics, Trinity College Dublin, College Green, Dublin 2, Ireland
- ⁶ National Research Council of Canada, Herzberg Astronomy & Astrophysics Research Centre, 5071 West Saanich Road, Victoria, BC V9E 2E7, Canada
- ⁷ Université Clermont Auvergne, CNRS/IN2P3, LPCA, F-63000 Clermont-Ferrand, France
- ⁸ DIRAC Institute, Department of Astronomy, University of Washington, 3910 15th Avenue NE, Seattle, WA 98195, USA
- ⁹ Aix Marseille Université, CNRS/IN2P3, CPPM, Marseille, France
- ¹⁰ Department of Physics, Duke University Durham, NC 27708, USA
- ¹¹ Institute of Astronomy and Kavli Institute for Cosmology, University of Cambridge, Madingley Road, Cambridge CB3 0HA, UK
- ¹² Institute of Space Sciences (ICE-CSIC), Campus UAB, Carrer de Can Magrans, s/n, E-08193 Barcelona, Spain.
- ¹³ Institut d'Estudis Espacials de Catalunya (IEEC), 08860 Castelldefels (Barcelona), Spain
- ¹⁴ Division of Physics, Mathematics & Astronomy, California Institute of Technology, Pasadena, CA 91125, USA
- ¹⁵ Deutsches Elektronen-Synchrotron DESY, Platanenallee 6, 15738 Zeuthen, Germany
- ¹⁶ Institut für Physik, Humboldt-Universität zu Berlin, Newtonstr. 15, 12489 Berlin, Germany
- ¹⁷ Caltech Optical Observatories, California Institute of Technology, Pasadena, CA 91125
- ¹⁸ The Oskar Klein Centre, Department of Astronomy, AlbaNova, SE-106 91 Stockholm, Sweden
- ¹⁹ Nordic Optical Telescope, Rambla José Ana Fernández Pérez 7, ES-38711 Breña Baja, Spain